Composite Structures 297 (2022) 115975

Contents lists available at ScienceDirect

Composite Structures

journal homepage: www.elsevier.com/locate/compstruct

Microbuckling behavior of unidirectional fiber-reinforced shape memory polymer composite undergoing compressive deformation

Hanxing Zhao [a,1], Tong Mu [a,1], Xin Lan [a,*], Liwu Liu [b], Yanju Liu [b], Jinsong Leng [a,*]

[a] Centre of Composite Materials and Structures, Harbin Institute of Technology (HIT), Harbin 150080, People's Republic of China
[b] Department of Astronautical Science and Mechanics, Harbin Institute of Technology (HIT), Harbin 150001, People's Republic of China

ARTICLE INFO

Keywords:
Microbuckling
Post-buckling
Viscoelasticity
Strain-attenuation

ABSTRACT

The microbuckling mechanics of unidirectional fiber-reinforced shape memory polymer composite (SMPC) with low fiber volume fraction were investigated, and the mechanical models were formulated considering the attenuation of shear strain in the resin matrix near the buckled fibers. We deduced the analytical expression of the attenuation function and the key parameters during the microbuckling process of SMPC, including the critical buckling wavelength and strain. The values determined by finite element analysis verified the accuracy of the above theoretical predictions. The nonlinear stress–strain relationship during the post-buckling process was also investigated. Additionally, the classical elastic–viscoelastic correspondence principle was established to determine the dynamic buckling behaviors of SMPC at different temperatures. The viscoelastic parameters of shape memory polymer (SMP) were obtained from the isothermal stress relaxation experiments, and then the variation of buckling wavelength with time at different temperatures was evaluated.

1. Introduction

The shape memory polymer (SMP) is a kind of smart material that can change its shape in response to external stimuli, including light, electricity, heat, magnetism, moisture, and pH [1–5]. The SMP can be deformed from the initial shape to the deformed shape, and the deformed shape can be fixed; under certain external stimuli, the SMP will reversibly recover from the deformed shape to its initial shape [6–10]. The shape memory process of SMP is a deformation cycle of "initial state- shape fixed state-shape recovery state". Compared with the shape memory alloy (SMA), the SMP has advantages as a kind of smart material, such as lightweight, low density, large deformation capacity, easy adjustment of the glass transition temperature (T_g), low cost, good processability, and so on [11,12]. However, the shortcoming of low modulus and strength of SMP limit its applications in spacecraft [13]. So, continuous fiber reinforced shape memory polymer composite (SMPC) is manufactured to overcome the above obstacles. Because of the high specific strength, modulus and unique shape memory performance, SMPCs are widely used in aerospace applications, such as space deployable hinges, trusses and antennas, etc., some of which have even been designed as the load-carrying components [14–18] to bearing the axial compressive loads. Therefore, the compressive behaviors of SMPC structures have become a key problem to be solved urgently.

Some achievements have been made in the research about compressive buckling behaviors of laminated plates. It is found out that the microbuckling of fibers in the compressive processes of laminated plates will lead to the ultimate failure of composite materials [19–21]. As early as 1960, Dow and Gruntfest proposed the fiber microbuckling mechanisms [22,23], and they firstly linked the longitudinal compressive strength of composite materials to the instability of fibers. On this basis, Rosen considered the fiber as a rigid slender cylinder embedded in the ideal elastic resin matrix, and pioneered a prediction model for the longitudinal compressive strength of the continuous fiber-reinforced polymer composites based on the microbuckling of fibers [24]. He proposed that the continuous fibers arranged in parallel would buckle under the compressive load, and two buckling modes might occur in the transverse direction (extension mode and shear mode), as shown in Fig. 1. The extension mode model showed the influence of the elastic moduli of resin and fiber on the longitudinal compressive buckling loads, but the predicted values were much higher than that of the experimental values [25]. In the meantime, the effect of the resin's shear modulus on the composite's longitudinal compressive buckling loads

* Corresponding authors.
E-mail addresses: lanxin@hit.edu.cn (X. Lan), lengjs@hit.edu.cn (J. Leng).
[1] These authors contributed equally to this study.

https://doi.org/10.1016/j.compstruct.2022.115975
Received 7 April 2022; Received in revised form 2 July 2022; Accepted 5 July 2022
Available online 14 July 2022

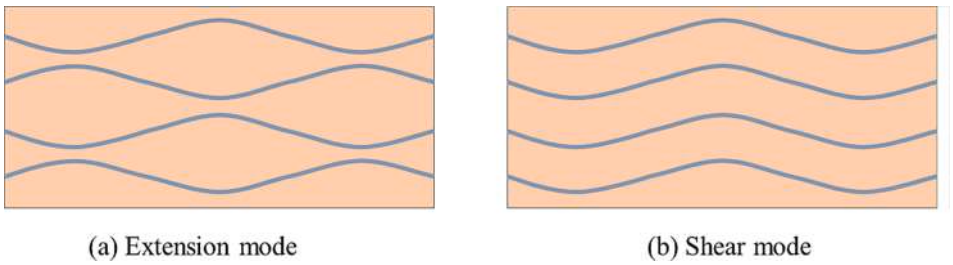

Fig. 1. Different microbuckling modes of continuous fiber-reinforced composites under compressive loading **(a)** extension mode, **(b)** shear mode.

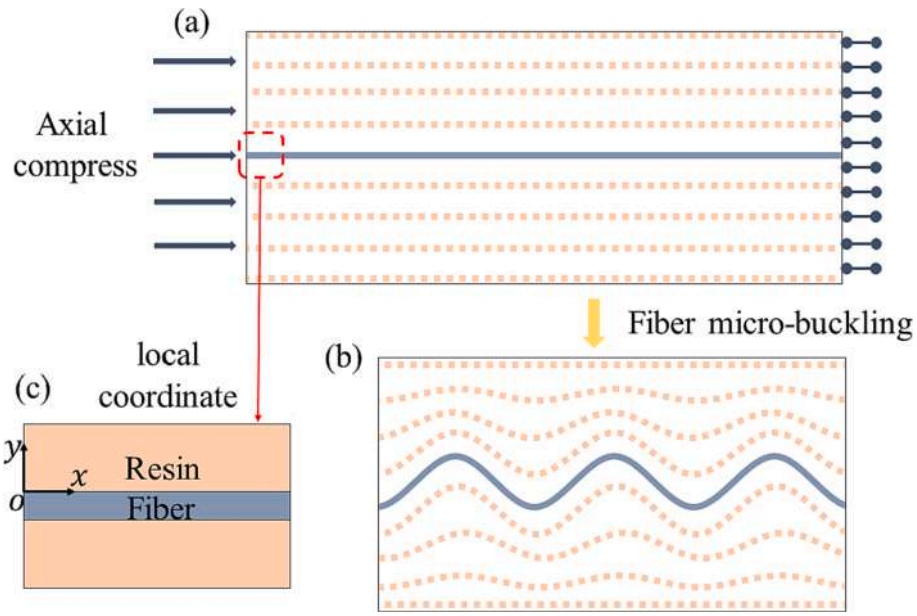

Fig. 2. The two-dimensional model of single-fiber reinforced SMPC (the blue line represents the fiber, while the pink dot lines represent the deformation of resin **(a)** single-fiber reinforced SMPC under axial compressive load, **(b)** the microbuckling state of single-fiber reinforced SMPC, **(c)** the local coordinate system.

was considered in the shear mode model, but the related material properties of the fibers were ignored, which was unreasonable. Subsequently, based on the properties of fibers, Lo and Chim modified Rosen's model [26], where the influence of the tensile modulus and in-plane shear modulus of the composite material on the longitudinal compressive performance was considered. Based on the theory of local buckling failure of fiber, they used Timoshenko's short beam theory [26] to analyze the stress of a single-fiber element. Xu and Reifsnider modeled the fiber as a short cylinder embedded in the ideal elastic resin matrix, and homogenized the fiber and resin based on the beam-on-elastic foundation model [27]. Lo and Chim thought that due to the limitation of the composite manufacturing process, there would be a small deviation angle between the directions of fiber alignment and the load, which was called the initial deviation angle of the fiber. The Lo-Chim model showed that fiber would exert large transverse shear stress on the resin matrix even with a very small initial deviation angle, resulting in a decrease in the in-plane shear modulus of the composite, which would lead to a significant reduction in the longitudinal compressive buckling load of the composite [28–30]. Campbell considered the buckling performances of single-fiber or multi-filament fibers in a square elastic matrix, and proposed a two-dimensional pure shear buckling model [31]. The calculated value of the buckling wavelength was in good agreement with the experiment result, but the critical buckling stress and strain were not reasonable.

The above buckling models were all based on the one-dimensional beam model or two-dimensional plane model. They all assumed that the shear strains were uniform around the buckled fibers, without considering the attenuation of strain in the matrix, which will result in deviations in the calculation results [32]. In addition, the matrix resins were considered as linear elastic materials, and the influence of temperature and viscoelasticity of resins were not considered. However, different from traditional fiber-reinforced polymer composites, the fiber volume fraction of SMPC is always low to take full advantage of the shape memory properties of SMP. As a result, the distance between fibers in SMPC is larger, which makes the attenuation of strain in the resin matrix must be considered. Besides, as a typical kind of temperature-sensitive and viscoelastic material, the mechanical properties of SMP have strong temperature and time dependences. With the increase of temperature, the resin matrix of SMPC will gradually change from the glassy state to the rubbery state, and Young's modulus ratio of fiber to resin will increase by two orders of magnitude; the relaxation modulus of SMP will gradually decrease with time, and the rate of descent is also temperature-dependent. Therefore, the microbuckling behaviors have a great difference between SMPC and traditional composites. The microbuckling wavelength and amplitude of SMPC will vary not only with the temperature, but also with time.

The main purpose of this paper is to study the microbuckling behaviors of SMPC with low fiber volume fractions. The attenuation effect of shear strain in matrix and the viscoelasticity of SMP are both considered in this paper, which can play a key role in the study of compressive microbuckling behaviors of unidirectional fiber-reinforced SMPCs with low fiber volume fractions. The structure of this paper is arranged as follows:

In the first part, the energy method is used to study the compressive

critical buckling and post-buckling behaviors of fiber reinforced linear elastic polymer composite. Single-fiber and multi-fiber reinforced composites are modeled respectively, and the key parameters during the whole nonlinear buckling process are analyzed. The classical elastic–viscoelastic correspondence principle is then established to solve the evolvement rule of the microbuckling wavelength of single-fiber reinforced SMPC with temperature and time. In the second part, the finite element method is used to model the single-fiber and multi-fiber reinforced composites to verify the accuracy of the proposed buckling theory. In the last part, the effects of fiber diameter, fiber volume fraction, temperature and Poisson's ratio of resin matrix on the critical buckling strain and nonlinear buckling stress–strain response are investigated. The time-dependent buckling wavelength can be determined by viscoelastic microbuckling model.

2. Theoretical analysis

The 2D compressive buckling model is established in this article to study the compressive microbuckling behavior of unidirectional fiber-reinforced SMPC. Single-fiber and multi-fiber reinforced composites are modeled respectively, and the viscoelasticity of the resin matrix is also taken into consideration.

2.1. Microbuckling mechanics of single-fiber reinforced SMPC

The microbuckling behaviors of single-fiber reinforced SMPC undergoing compressive deformation are firstly conducted, and the corresponding two-dimensional model is established as shown in Fig. 2. Assuming that a single fiber is embedded in an infinite resin matrix, where fiber is assumed to be beam element and resin is assumed to be shell element. The longitudinal displacement on one end is constrained and subjected to the axial compressive force at the other end, resulting in the microbuckling of the fiber. It should be noted that if the fiber is modeled with a circular cross-section, the strain distribution of the resin matrix around the fiber will be uneven, which will make this problem difficult to be solved. Therefore, to simplify the calculation, the influence of the shape of the fiber's cross-section will not be considered hereafter. In the following of this paper, the cross-section of the fiber is equivalent to a square section with a side length d, where d is the equivalent diameter of the fiber, and has the following relationship with the actual radius r of the fiber.

$$d^2 = \pi r^2 \# \tag{1}$$

In the local coordinate system as shown in Fig. 2(c), the fiber buckling deformation is assumed to have the following expression:

$$y = A_f \cos\left(\frac{\pi x}{\lambda}\right) \# \tag{2}$$

where λ and A_f are the half-wavelength and amplitude of the buckled fiber, respectively.

The macroscopic strain of the composite plate along the x-axial in the compressive process can be calculated as.

$$\varepsilon = \frac{1}{2\lambda}\int_0^{\lambda}\left(\sqrt{(dx)^2 + (dy)^2} - dx\right)dx \approx \frac{1}{2\lambda}\int_0^{\lambda}\left(\frac{dy}{dx}\right)^2 dx = \frac{\pi^2}{4\lambda^2}{A_f}^2 \# \tag{3}$$

Therefore, it can be considered that the buckling amplitude A_f is a function of the half-wavelength λ and the macroscopic compressive strain ε, i.e.

$$A_f = \frac{2}{\pi}\lambda\sqrt{\varepsilon} \# \tag{4}$$

Assuming that the fiber is incompressible, so only the bending strain energy of the fiber need to be considered. The strain energy of a fiber with the length of λ under small deformation is.

$$U_{f,s} = \frac{EI}{2}\int_0^{\lambda}\left(\frac{\partial^2 y}{\partial x^2}\right)^2 dx = \frac{\pi^2 E_f I_f}{\lambda}\varepsilon \# \tag{5}$$

The average strain energy over per unit length range of the buckled fiber is.

$$U_f = \frac{U_{f,s}}{\lambda} = \frac{\pi^2 E_f I_f}{\lambda^2}\varepsilon \# \tag{6}$$

where E_f and I_f are the longitudinal Young's modulus and the moment of inertia of the fiber, and $I_f = d^4/12$.

It is assumed that the fiber and resin matrix are tightly bonded, so the deformation of the resin at the joint place has the same expression with fiber, i.e.

$$y|_{y=0} = A_f \cos\left(\frac{\pi x}{\lambda}\right) \# \tag{7}$$

While SMP is a typical temperature-sensitive material, whose modulus changes dramatically with temperature. The modulus of resin matrix will be much lower than that of fiber at relatively high temperatures (around the glass transition temperature, T_g). Just like dropping a stone into water, the farther away from the stone, the smaller the ripples in the water will be. Therefore, the displacement of resin matrix will be inhomogeneous along the y-direction, which will attenuate with the increase of the distance between fiber and resin. As shown in Fig. 2(b), at a sufficient distance from the fiber, the resin will hardly deform, which can also be observed in the following finite element analysis (Fig. 6). So, the attenuation function $\chi(|y|)$ is introduced in this article to describe this phenomenon, where $|y|$ is the perpendicular distance from a point in the matrix resin to the surface of the fiber. $\chi(|y|)$ satisfies the following two boundary conditions.

$$\chi(0) = 1 \# \tag{8}$$

$$\chi(\infty) = 0 \# \tag{9}$$

Then, the displacements of the matrix resin at any point are.

$$u = \varepsilon x + const \# \tag{10}$$

$$v = A_f \chi(|y|)\cos\left(\frac{\pi x}{\lambda}\right) \# \tag{11}$$

$$w = 0 \# \tag{12}$$

As for the two-dimensional system shown in Fig. 2, only the upper matrix is considered, i.e., $y > 0$. It is assumed that $const = 0$, the displacement of the matrix resin can be expressed as.

$$[u \quad v] = \left[\varepsilon x \quad \frac{2\sqrt{\varepsilon}\lambda}{\pi}\chi(y)\cos\left(\frac{\pi x}{\lambda}\right)\right] \# \tag{13}$$

So, the strain of matrix resin is.

$$\varepsilon = \begin{bmatrix} \varepsilon & -\sqrt{\varepsilon}\chi(y)\sin\left(\frac{\pi x}{\lambda}\right) \\ -\sqrt{\varepsilon}\chi(y)\sin\left(\frac{\pi x}{\lambda}\right) & \frac{2\sqrt{\varepsilon}\lambda\cos\left(\frac{\pi x}{\lambda}\right)\chi'(y)}{\pi} \end{bmatrix} \# \tag{14}$$

In this paper, the resin matrix is simulated as the shear-lag model and only the shear deformation is considered, so the strain energy density of the matrix resin is.

$$\psi = \frac{G}{2}\left(\varepsilon - \frac{1}{3}\mathrm{tr}\varepsilon\right) : \left(\varepsilon - \frac{1}{3}\mathrm{tr}\varepsilon\right) \# \tag{15}$$

The $\frac{1}{3}\mathrm{tr}\varepsilon$ term is ignored, so the strain energy density of the matrix resin can be expressed as.

$$\psi = \frac{G}{2}\varepsilon : \varepsilon = \overline{U}_{xx} + \overline{U}_{yy} + \overline{U}_{xy} = \frac{G}{2}\varepsilon_{xx}^2 + \frac{G}{2}\varepsilon_{yy}^2 + G\varepsilon_{xy}^2 \# \tag{16}$$

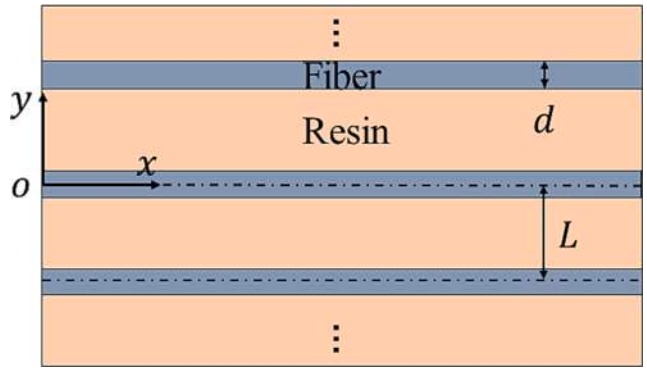

Fig. 3. The two-dimensional model of multi-fiber reinforced SMPC.

$$\overline{U}_{xx} = \frac{G}{2}\varepsilon^2 \# \tag{17}$$

$$\overline{U}_{yy} = \frac{2\lambda^2 G}{\pi^2}\chi'(y)^2 cos^2\left(\frac{\pi x}{\lambda}\right)\varepsilon \# \tag{18}$$

$$\overline{U}_{xy} = G\chi(y)^2 sin^2\left(\frac{\pi x}{\lambda}\right)\varepsilon \# \tag{19}$$

where $G = E_m/2(1+\nu)$ is the shear modulus of the resin, ν is the Poisson's ratio of the resin, $\overline{U}_{xx}$, $\overline{U}_{xy}$ and $\overline{U}_{yy}$ are the strain energy density components of the resin.

Define $\psi_0 = \overline{U}_{yy} + \overline{U}_{xy}$, which represents the effect of buckled fiber on the strain energy density of matrix, excluding the uniform strain energy density of the matrix $\overline{U}_{xx}$.

The uniform strain energy per unit length of the matrix is.

$$U_{xx} = \overline{U}_{xx} d(b-d) = \frac{G}{2}\varepsilon^2 d(b-d) \# \tag{20}$$

where b is the overall width of SMPC.

Assuming that the attenuation function is an exponential function (the rationality of this hypotheses will be subsequently verified by FEA).

$$\chi(y) = e^{-ky} \# \tag{21}$$

The strain energy density ψ_0 is integrated over per unit length range of the buckled fiber.

$$U_{m0} = 2\frac{d}{\lambda}\int_0^{\infty}\int_0^{\lambda}\psi_0 dxdy = 4G\left(\frac{k\lambda^2}{2\pi^2} + \frac{1}{4k}\right)\varepsilon d \# \tag{22}$$

So, the strain energy per unit length of the whole system can be calculated as.

$$U = U_{xx} + U_{m0} + U_f = \frac{G}{2}d(b-d)\varepsilon^2 + \left(\frac{\pi^2 E_f I_f}{\lambda^2} + \frac{2k\lambda^2 G}{\pi^2}d + \frac{G}{k}d\right)\varepsilon \# \tag{23}$$

The coefficient of the attenuation function can be conducted through the principle of minimum strain energy.

$$\frac{\partial U}{\partial k} = 0 \# \tag{24}$$

$$k = \frac{\pi}{\sqrt{2}\lambda} \# \tag{25}$$

It can be seen from Eq. (25) and Eq. (21) that with the decrease of the half-wavelength of the fiber, the attenuation rate of strain in resin matrix will become faster.

Substitute Eq. (25) into Eq. (23) derive the following expression.

$$U = \frac{G}{2}d(b-d)\varepsilon^2 + 2\left(\frac{\pi^2 E_f I_f}{2\lambda^2} + \frac{\sqrt{2}\lambda G}{\pi}d\right)\varepsilon \# \tag{26}$$

Similarly, the half-wavelength can be calculated according to the principle of minimum strain energy.

$$\frac{\partial U}{\partial \lambda} = 0 \# \tag{27}$$

$$\lambda = \frac{\pi}{\sqrt[6]{2}}\sqrt[3]{\frac{E_f I_f}{\mu d}} \approx 1.54 d\sqrt[3]{\frac{E_f(1+\nu)}{E_m}} \# \tag{28}$$

It is worth noting that the above buckling analysis is a linear buckling analysis, and only basic information about the critical buckling wavelength can be obtained. However, the critical buckling state of the composite cannot be observed in the experiment. We can only observe that the mechanical equilibrium path (load–displacement curve) of the composite material will bifurcate when buckling. After the bifurcation point, the material will not completely lose its load carrying capacity, but partially recover its bearing capacity and enter the secondary equilibrium path. Therefore, the mechanical behavior of the composite material in the whole process of buckling may be highly nonlinear. As a consequence, if we want to obtain the mechanical response of the composite material in the whole buckling process, we must study its nonlinear buckling behavior, that is, the post-buckling behavior.

It is emphasized again that since the small deformation assumption is considered in this paper, the buckling wavelength can be regarded as unchanged during the whole nonlinear buckling process, then the critical buckling strain of this single-fiber reinforced SMPC can be deduced from this assumption. The pre-buckling state is represented by a subscript "0", while the post-buckling state is represented by a subscript "1".

In the pre-buckling state, no buckling deformation occurs in the fiber, so the strain energy of the SMPC (per unit length) can be expressed as.

$$U_0 = \frac{1}{2}E_e\varepsilon_0^2 bd \# \tag{29}$$

where.

$$E_e = \frac{d}{b}E_f + \left(1 - \frac{d}{b}\right)E_m \# \tag{30}$$

is the equivalent modulus of the single-fiber reinforced composite.

In the post-buckling state, the strain energy of the SMPC (per unit length) can be expressed as.

$$U_1 = \frac{G}{2}d(b-d)\varepsilon_1^2 + 2\left(\frac{\pi^2 E_f I_f}{2\lambda^2} + \frac{\sqrt{2}\lambda G}{\pi}d\right)\varepsilon_1 \# \tag{31}$$

So, the critical buckling strain $\varepsilon_{critical}$ can be calculated as $U_0 = U_1$ and $\varepsilon_0 = \varepsilon_1 = \varepsilon_{critical}$, i.e.

$$\frac{1}{2}E_e\varepsilon_{critical}^2 bd = \frac{G}{2}d(b-d)\varepsilon_{critical}^2 + 2\left(\frac{\pi^2 E_f I_f}{2\lambda^2} + \frac{\sqrt{2}\lambda G}{\pi}d\right)\varepsilon_{critical} \# \tag{32}$$

$$\varepsilon_{critical} = \frac{4}{(E_e+G)bd - Gd^2}\left(\frac{\pi^2 E_f I_f}{2\lambda^2} + \frac{\sqrt{2}\lambda G}{\pi}d\right) \# \tag{33}$$

Then, the stress–strain response of the single-fiber reinforced composite material in the whole post-buckling process can be calculated. The partial derivative of the strain energy density before and after buckling with respect to strain is equal to the stress in the whole nonlinear buckling process, i.e.

$$\sigma = \begin{cases} \dfrac{\partial U_0}{db\partial\varepsilon}, \varepsilon \le \varepsilon_{critical} \\ \dfrac{\partial U_1}{bd\partial\varepsilon}, \varepsilon > \varepsilon_{critical} \end{cases} \# \tag{34}$$

$$\sigma = \begin{cases} \left[\frac{d}{b}E_f + \left(1-\frac{d}{b}\right)E_m\right]\varepsilon, \varepsilon \le \varepsilon_{critical} \\ G\left(1-\frac{d}{b}\right)\varepsilon + 2\left(\frac{\pi^2 E_f I_f}{2db\lambda^2} + \frac{\sqrt{2}\lambda G}{\pi b}\right), \varepsilon > \varepsilon_{critical} \end{cases} \# \tag{35}$$

It can be seen that the stress is a piecewise function in the whole nonlinear buckling process, and the strain corresponding to bifurcation point is the critical buckling strain $\varepsilon_{critical}$.

2.2. Microbuckling mechanics of multi-fiber reinforced SMPC

The uniaxial compressive buckling behavior of a single-fiber reinforced SMPC was discussed in the above section. It can be seen that the buckling wavelength of the fiber is only related to the basic mechanical properties of the fiber and resin. The uniaxial compressive buckling behavior of uniformly distributed multi-fiber reinforced SMPC is discussed and analyzed below. The two-dimensional model is established as shown in Fig. 3. Assuming that fibers are evenly distributed in the resin matrix, the equivalent diameter of the fiber is d, and the distance between the central axes of adjacent fibers is L. The volume fraction of the fibers can be expressed as $V_f = d/L$.

It can be seen from the figure that the ordinates of the initial positions of fibers' central axes are.

$$y_f = \cdots, -2L, -L, 0, L, 2L, \cdots \# \tag{36}$$

As the fibers in the two-dimensional model are arranged periodically along the y-axis, so we can represent the resin in the whole model by the resin between two adjacent fibers, i.e., $-d/2 < y < L-d/2$. In addition, the microbuckling process is a small deformation process, and the resin matrix is the same with that of the single-fiber reinforced SMPC, so the attenuation function will not change.

The superposition principle is firstly used to calculate the effect of fibers at $y_f = \cdots, -2L, -L, 0$ on the strain at a point $y_m = y$ of the matrix resin. It should be noted that the linear superposition method is directly used in this article to calculate the strain energy of the matrix, without considering the obstruction of strain energy propagation by adjacent fibers. The resulting strain energy will be greater than the actual value, especially when the fiber volume fraction is high. Therefore, the calculation method and strain energy superposition assumption adopted in this paper are only applicable to the SMPC with fiber volume fraction less than 5 %.

As for the fiber at $y_f = 0$, the distance from the upper surface of the fiber to the point $y_m = y$ is.

$$h = y - \frac{d}{2} \# \tag{37}$$

So, the strains can be calculated as.

$$\varepsilon_{yy}^{0} = -\sqrt{\varepsilon}\chi\left(y-\frac{d}{2}\right)\sin\left(\frac{\pi x}{\lambda}\right)\# \tag{38}$$

$$\varepsilon_{xy}^{0} = \frac{2\sqrt{\varepsilon}\lambda}{\pi}\chi'\left(y-\frac{d}{2}\right)\cos\left(\frac{\pi x}{\lambda}\right)\# \tag{39}$$

In a similar way, as for the fibers at $y_f = -nL(n>0)$, the distance from the upper surface of the fibers to this point is.

$$h = y + nL - \frac{d}{2} \# \tag{40}$$

The strains can be calculated as.

$$\varepsilon_{yy}^{-n} = -\sqrt{\varepsilon}\chi\left(y+nL-\frac{d}{2}\right)\sin\left(\frac{\pi x}{\lambda}\right)\# \tag{41}$$

$$\varepsilon_{xy}^{-n} = \frac{2\sqrt{\varepsilon}\lambda}{\pi}\chi'\left(y+nL-\frac{d}{2}\right)\cos\left(\frac{\pi x}{\lambda}\right)\# \tag{42}$$

Therefore, it can be deducted that the influence of all fibers at $y_f \le 0$ on strains at this position are.

$$\varepsilon_{yy}^{lower} = \sum_{n=-\infty}^{0}\varepsilon_{yy}^{n} = \frac{\sqrt{\varepsilon}e^{\frac{\pi(d-2y)}{2\sqrt{2}\lambda}}}{e^{\frac{\sqrt{2}L}{\lambda}}-1}sin\left(\frac{\pi x}{\lambda}\right)\# \tag{43}$$

$$\varepsilon_{xy}^{lower} = \sum_{n=-\infty}^{0}\varepsilon_{xy}^{n} = \sqrt{2}\,\frac{\sqrt{\varepsilon}e^{\frac{\pi(d-2y)}{2\sqrt{2}\lambda}}}{e^{\frac{\sqrt{2}L}{\lambda}}-1}cos\left(\frac{\pi x}{\lambda}\right)\# \tag{44}$$

Then, as for the fibers at $y_f = nL(n>0)$, the distance from the lower surface of the fibers to this point is.

$$h = nL - y - \frac{d}{2} \# \tag{45}$$

The strains can be calculated as.

$$\varepsilon_{yy}^{0} = -\sqrt{\varepsilon}\chi\left(nL-y-\frac{d}{2}\right)\sin\left(\frac{\pi x}{\lambda}\right)\# \tag{46}$$

$$\varepsilon_{xy}^{0} = \frac{2\sqrt{\varepsilon}\lambda}{\pi}\chi'\left(nL-y-\frac{d}{2}\right)\cos\left(\frac{\pi x}{\lambda}\right)\# \tag{47}$$

So, it can be deducted that.

$$\varepsilon_{yy}^{upper} = \sum_{n=1}^{\infty}\varepsilon_{yy}^{n} = -\frac{\sqrt{\varepsilon}e^{\frac{\pi(d+2y)}{2\sqrt{2}\lambda}}}{e^{\frac{\sqrt{2}L}{\lambda}}-1}sin\left(\frac{\pi x}{\lambda}\right)\# \tag{48}$$

$$\varepsilon_{xy}^{upper} = \sum_{n=1}^{\infty}\varepsilon_{xy}^{n} = -\sqrt{2}\,\frac{\sqrt{\varepsilon}e^{\frac{\pi(d+2y)}{2\sqrt{2}\lambda}}}{e^{\frac{\sqrt{2}L}{\lambda}}-1}cos\left(\frac{\pi x}{\lambda}\right)\# \tag{49}$$

Therefore, the strain at $-d/2 < y < L-d/2$ can be calculated through the superposition principle.

$$\varepsilon_{yy} = \varepsilon_{yy}^{lower} + \varepsilon_{yy}^{upper} = \frac{\sqrt{\varepsilon}}{e^{\frac{\sqrt{2}L}{\lambda}}-1}\left[e^{\frac{\pi(d-2y)}{2\sqrt{2}\lambda}} - e^{\frac{\pi(d+2y)}{2\sqrt{2}\lambda}}\right]\sin\left(\frac{\pi x}{\lambda}\right)\# \tag{50}$$

$$\varepsilon_{xy} = \varepsilon_{xy}^{lower} + \varepsilon_{xy}^{upper} = -\sqrt{2}\,\frac{\sqrt{\varepsilon}}{e^{\frac{\sqrt{2}L}{\lambda}}-1}\left[e^{\frac{\pi(d-2y)}{2\sqrt{2}\lambda}} - e^{\frac{\pi(d+2y)}{2\sqrt{2}\lambda}}\right]\cos\left(\frac{\pi x}{\lambda}\right)\# \tag{51}$$

ψ_0 and U_{m0} can be expressed as.

$$\begin{aligned}\Psi_0 &= \overline{U}_{yy} + \overline{U}_{xy} = \frac{G}{2}\varepsilon_{yy}^2 + 2\times\frac{G}{2}\varepsilon_{xy}^2 \\ &= \frac{G}{4}e^{\frac{\pi(d-2y)}{\sqrt{2}\lambda}}\left(3\cos\left(\frac{2\pi x}{\lambda}\right)+5\right)\left(\frac{e^{\frac{\sqrt{2}\pi y}{\lambda}}-1}{e^{\frac{\sqrt{2}L}{\lambda}}-1}\right)^2\varepsilon\#\end{aligned} \tag{52}$$

$$\begin{aligned}U_{m0} &= d\frac{1}{\lambda}\int_{d/2}^{L-d/2}\int_{0}^{\lambda}\psi_0 dxdy \\ &= \frac{5dG}{8\pi\left(e^{\frac{\sqrt{2}L}{\lambda}}-1\right)^2}\left(4\pi d e^{\frac{\sqrt{2}\pi d}{\lambda}} - \sqrt{2}\lambda e^{\frac{\sqrt{2}\pi d}{\lambda}} - \sqrt{2}\lambda e^{\frac{\sqrt{2}\pi(d-L)}{\lambda}} - 4\pi L e^{\frac{\sqrt{2}\pi d}{\lambda}} + \sqrt{2}\lambda + \sqrt{2}\lambda e^{\frac{\sqrt{2}\pi L}{\lambda}}\right)\varepsilon\#\end{aligned} \tag{53}$$

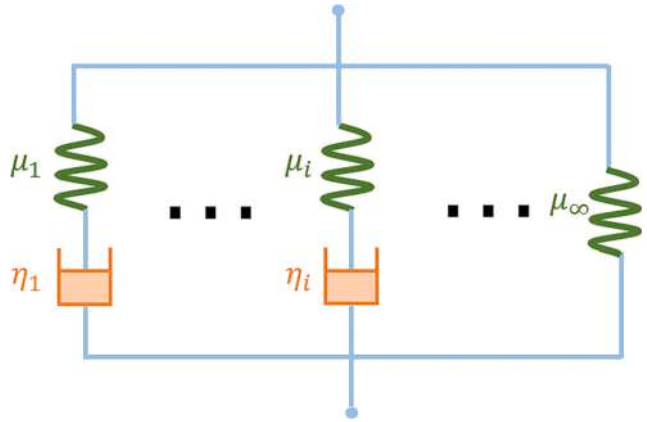

Fig. 4. The generalized Maxwell model of the viscoelastic resin.

The whole strain energy per unit length of the composite is $U = U_{xx} + U_{m0} + U_f$, where $U_{xx} = G\varepsilon^2 d(L-d)/2$, $U_f = \pi^2 E_f I_f \varepsilon/\lambda^2$.

The half-wavelength can be calculated according to the principle of minimum strain energy (numerical solution).

$$\frac{\partial U}{\partial \lambda} = 0\# \tag{54}$$

The material parameters are normalized as dimensionless parameters, i.e.

$$\alpha = \frac{E_f I_f}{Gd^4} = \frac{(1+v)E_f}{6E_m}, \beta = \frac{\lambda}{d}, \phi = \frac{d}{L} = V_f\# \tag{55}$$

The whole strain energy can be expressed as.

$$U = \frac{(1-\phi)Gd^2}{2\phi}\varepsilon^2 + \frac{Gd^2}{8\pi}\zeta\varepsilon\# \tag{56}$$

where.

$$\zeta = \frac{8\pi^3\alpha}{\beta^2} + \frac{5\left(4\pi e^{\frac{\pi}{\sqrt{2}\beta}}(\phi-1) - \sqrt{2}\,e^{\frac{\sqrt{2}\pi}{\beta}}\beta\phi - \sqrt{2}\beta\phi e^{\frac{\sqrt{2}\pi(\phi-1)}{\beta\phi}} + \sqrt{2}\beta\phi e^{\frac{\sqrt{2}\pi}{\beta\phi}} + \sqrt{2}\beta\phi\right)}{\phi\left(e^{\frac{\pi}{\sqrt{2}\beta\phi}} - 1\right)^2}\# \tag{57}$$

ζ is a dimensionless parameter which is related to the shear strain energy of resin matrix and the bending strain energy of fibers. It should be noted that ζ is only related to the material parameters and fiber volume fraction.

Similar to the single-fiber reinforced composite, the strain energy of the multi-fiber reinforced SMPC in the pre-buckling state (per unit length) can be expressed as.

$$U_0 = \frac{1}{2}E_e\varepsilon^2 dL\# \tag{58}$$

where $E_e = V_f E_f + (1-V_f)E_m$ is the equivalent modulus of composite.

In the post-buckling state, the strain energy of the SMPC (per unit length) can be expressed as.

$$U_1 = \frac{G}{2\phi}\varepsilon^2 d^2(1-\phi) + \frac{d^2 G}{8\pi}\zeta\varepsilon\# \tag{59}$$

So, the critical buckling strain $\varepsilon_{critical}$ can be calculated as $U_0 = U_1$, i.e.

$$\frac{1}{2\phi}E_e\varepsilon^2 d^2 = \frac{G}{2\phi}\varepsilon^2 d^2(1-\phi) + \frac{d^2 G}{8\pi}\zeta\varepsilon\# \tag{60}$$

$$\varepsilon_{critical} = \frac{G}{4\pi[E_e - G(1-\phi)]}\phi\zeta\# \tag{61}$$

The stress–strain response can be calculated as.

$$\sigma = \begin{cases} \dfrac{\partial U_0}{dL\partial\varepsilon}, \varepsilon \le \varepsilon_{critical} \\ \dfrac{\partial U_1}{dL\partial\varepsilon}, \varepsilon > \varepsilon_{critical} \end{cases}\# \tag{62}$$

$$\sigma = \begin{cases} \left[V_f E_f + (1-V_f)E_m\right]\varepsilon, \varepsilon \le \varepsilon_{critical} \\ (1-V_f)G\varepsilon + \dfrac{G}{8\pi}\zeta V_f, \varepsilon > \varepsilon_{critical} \end{cases}\# \tag{63}$$

2.3. Considering the viscoelasticity of SMP

The resins are assumed to be linear elastic materials in the above calculation process, without considering the viscoelasticity of SMPs. However, as a typical shape memory material, the modulus of SMP has strong temperature and time dependence. The corresponding critical buckling and post-buckling behaviors of SMPC will vary not only with temperature but also with time. So, the viscoelasticity of SMP should also be taken into consideration. In this part, the SMP is assumed to be isotropic, linear viscoelastic, and the Poisson's ratio is assumed to be invariable with the change of temperature. Under isothermal conditions, the influence of thermal expansion coefficient can be ignored, so the corresponding viscoelastic constitutive relation of the composite materials is.

$$\tau_{xy}(t) = \frac{1}{2(1+v)}\int_{-\infty}^{t}\mu(t-\tau)\frac{\partial\gamma_{xy}(\tau)}{\partial\tau}d\tau\# \tag{64}$$

where $\mu(t)$ is the viscoelastic relaxation modulus. The glassy modulus $\mu(0) = \mu_0$, and rubbery modulus $\mu(\infty) = \mu_\infty$, correspondingly. The Laplace transform of Eq. (64) is.

$$\bar{\tau}_{xy}(s) = \frac{1}{2(1+v_r)}s\bar{\mu}(s)\bar{\gamma}_{xy}(s)\# \tag{65}$$

where s is the transform variable, and a bar over a variable designates its Laplace transform.

Similarly, since the wavelength of the fiber also varies with time, the Laplace transform of the fiber waveform is.

$$\bar{y}(s) = A\cos\left(\frac{\pi x}{\bar{\lambda}(s)}\right)\# \tag{66}$$

Substituting Eq. (65) and Eq. (66) into Eq. (26) and Eq. (27), the corresponding half-wavelength of the fiber can be obtained through the similar energy minimum principle.

$$\bar{\lambda}(s) = \sqrt[6]{2}\pi\sqrt[3]{\frac{E_f I_f(1+v)}{s\bar{\mu}(s)d}} = m\sqrt[3]{\frac{1}{s\bar{\mu}(s)}}\# \tag{67}$$

where.

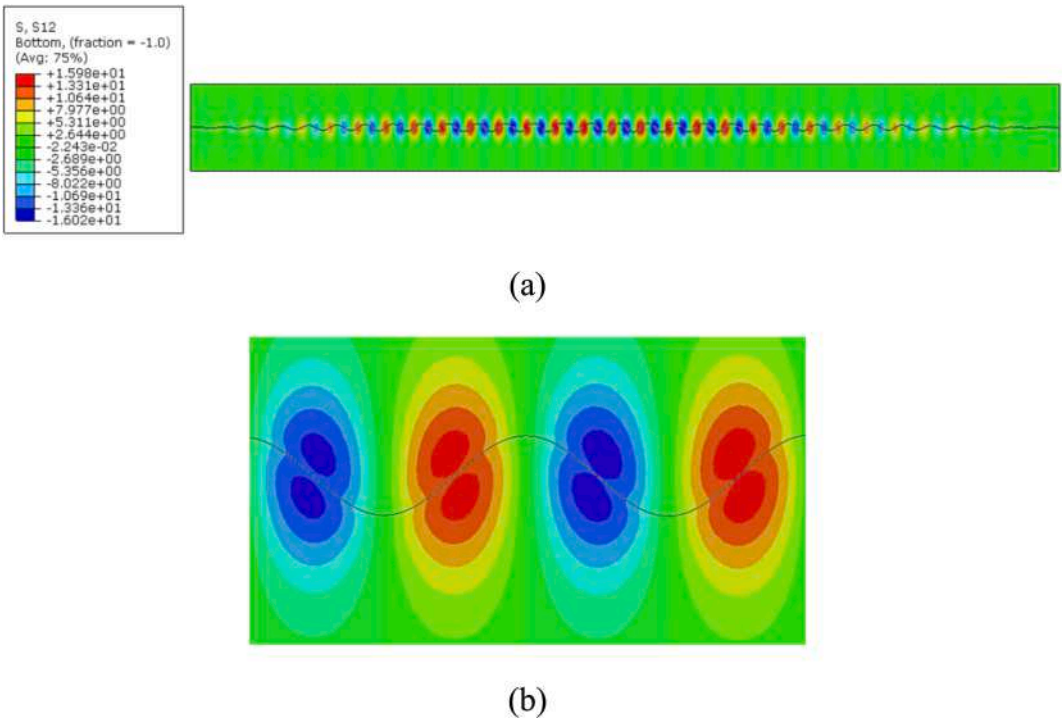

Fig. 5. Shear stress contour of single-CF reinforced composite at 100°C from the FEA result (deformation scale 1:10) **(a)** the shear stress contour, **(b)** a close-up plot of the shear stress distribution near the fiber.

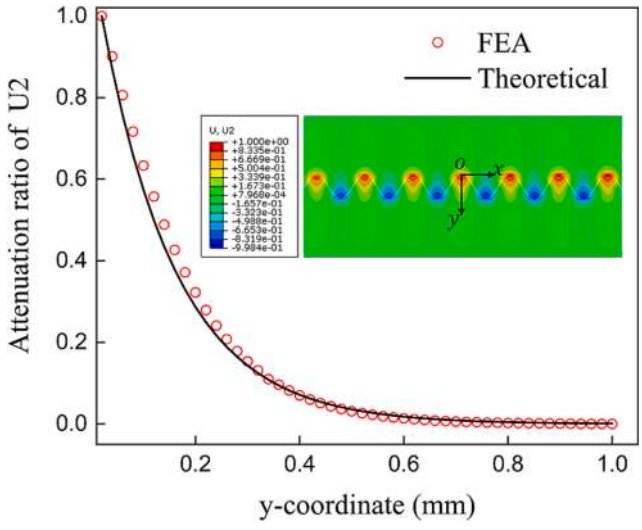

Fig. 6. Theoretical and FEA results of the attenuation ratio of displacement in resin matrix in the y-direction (single-CF reinforced composite at 100 °C in the critical buckling state).

Table 1
Parameters of the FEA model of single-fiber reinforced composite.

Material	Element	Cross profile	Young's Modulus (GPa)	Poisson's ratio
Epoxy	CPS4R	Plane stress thickness (The same with fiber)	Change with temperatures	0.3
CNF	B21	$62\mu m \times 62\mu m$ rectangular	5	0.5
CF	B21	$6.2\mu m \times 6.2\mu m$ rectangular	230	0.5

$$m = \sqrt[6]{2}\pi\sqrt[3]{\frac{E_f I_f (1+\nu)}{d}}\# \tag{68}$$

Let $D(t) = d\lambda/dt$, the corresponding Laplace transform is.

$$\overline{D}(s) = s\overline{\lambda}(s) - \lambda_0\# \tag{69}$$

where λ_0 is the initial buckling half-wavelength. Substituting Eq. (69) into Eq. (67), $\overline{D}(s)$ can be expressed as.

$$\overline{D}(s) = \frac{m^3}{\overline{\mu}(s)}\overline{\lambda}^{-2}(s) - \lambda_0\# \tag{70}$$

The inverse Laplace transform of Eq. (70) leads to an integral–differential equation governing the growth of the perturbation, and the numerical methods are taken hereinafter.

As shown in Fig. 4, according the generalized Maxwell model, the viscoelastic relaxation modulus $\mu(t)$ can be expressed as.

$$\mu(t) = \mu_\infty + \sum_i \mu_i \exp(-p_i t)\# \tag{71}$$

where p_i is the relaxation parameter of one branch, and $p_i = \mu_i/\eta_i$. The Laplace transform of $\mu(t)$ is.

$$\overline{\mu}(s) = \frac{\mu_\infty}{s} + \sum_i \frac{\mu_i}{s+p_i}\# \tag{72}$$

Only the first two terms of Eq. (72) are used, so it can be rewritten as.

$$\overline{\mu}(s) = \frac{\mu_\infty}{s} + \frac{\mu_1}{s+p_1}\# \tag{73}$$

$$\mu_1 = \mu_0 - \mu_\infty$$

The parameters μ_1, μ_∞ and p_1 at different temperatures can be obtained by the following isothermal stress relaxation experiments of SMP. So, by substituting Eq. (73) into Eq. (70), the numerical solution of $D(t)$ can be easily obtained by inverse Laplace transform. From this, the variation rate of buckling wavelength with time of single-fiber reinforced SMPC at different temperatures can be calculated. It is worth

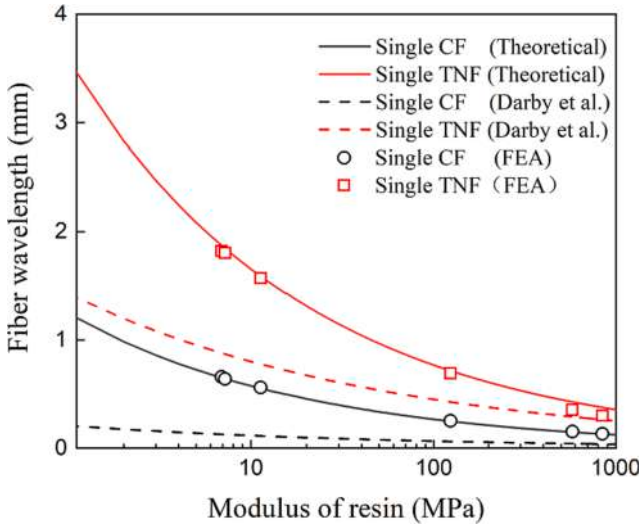

Fig. 7. The critical buckling wavelength of single-CF reinforced composite at 100 °C as a function of E_m obtained from theoretical analysis, FEA and literature [33].

Table 2
The critical buckling wavelength of single-fiber reinforced composite from theoretical analysis and literatures [20,33,34].

Diameter of fiber (um)	Young's modulus of fiber (GPa)	Shear modulus of matrix (MPa)	Experimental wavelength (mm)	Theoretical wavelength (mm)	Darby [33] (mm)
7	230	18.46	0.27 ± 0.13 [20]	0.35	0.16
50	5.6	0.043	5.4 ± 0.2[34]	5.5	2.04

noting that the variation trend of buckling half-wavelength of fiber with time $\lambda(t)$ at different temperatures can also be obtained by simple numerical integration of $D(t)$. The evolutions of buckling wavelength at different temperatures are shown in Section 4.3.

3. Verification of the theoretical analysis

The accuracy of the theoretical models will be verified by the commercial finite element software Abaqus 6.14. The FEA is used to model the single-fiber and multi-fiber reinforced composites to verify the reliability of the attenuation function. Then, the critical buckling wavelength calculated theoretically is compared with the FEA and literature results to verify the accuracy of the proposed theory.

3.1. Single-fiber reinforced composite

Firstly, the finite element model of the single-fiber reinforced composite is established. As can be seen in Fig. 5, the shear stress of the resin matrix near the buckled fiber is extremely high and the value fluctuates periodically. Although the buckling wavelength of the fiber does not change in the whole model, its amplitude will attenuate at the ends of the model, so the periodic boundary conditions (PBC) are not applicable to critical buckling analysis. Therefore, the axial dimension of the model must be long enough to include sufficient microbuckling waves to ensure the accuracy of FEA. In addition, the width of the model should be much larger than the equivalent diameter of the fiber to eliminate the influence of boundary constraints. Taking the above factors into consideration, the overall size of the model should be $20mm \times 2mm$. Other parameters of the finite element model are shown in Table 1, in which the modulus of resin will change with the temperature, and the specific values are shown in Table S1 (Supplemental File). As shown in Section S2.1 (Supplemental File), the moduli of SMP at different temperatures are determined through the isothermal compression experiments, and it is assumed that the modulus of fiber does not vary with temperature.

The critical buckling behaviors of the single carbon fiber (CF, T300 carbon fiber, Toray Industries, Inc, Japan) and single carbon nanofiber (CNF, TNF 400, Chengdu Organic Chemicals Co., ltd, China) reinforced composites at different temperatures are simulated by FEA after the dimensions and material parameters of the finite element models are determined. The linear perturbation-buckling analysis step is used to determine the critical buckling wavelength, and the subspace algorithm is adopted to guarantee the accuracy.

First of all, the feasibility and accuracy of the attenuation function $\chi(y)$ should be verified. Fig. 6 shows the comparison of theoretical and simulation results of the attenuation ratio of displacement in the resin matrix. It can be seen from the y-directional displacement contour that the displacement of resin will decay with the increase of y. Then, a coordinate system oxy is established on one wave peak of the fiber, and the attenuation ratio of the resin's displacement in the y-direction at $x = 0$ is calculated through the finite element displacement contours. The comparison with the theoretical results is also shown in this figure, it can be seen that the finite element results are in good agreement with the theoretical results. It can also be seen from Fig. 6 that the displacement of resin will decay with the increase of y, which will even gradually approach 0 when $y > 0.5$mm. So, if the displacement-attenuation of the resin is not taken into account, the results may not be affected much when the space between adjacent fibers is relatively small; while with the increase of the distance between adjacent fibers, the results will be more and more inaccurate. That is to say, when the fiber volume fraction is small, the attenuation of strain in the resin must be taken into consideration.

The Mises-stress contours of pure fiber and single CF and CNF reinforced composite at different temperatures are shown in Appendix A. As can be seen from Fig. A, the critical buckling modes of pure CF and CNF are both Euler buckling modes, indicating that the strain energy of a buckled ideal elastic beam is always minimum in Euler buckling mode. When the fiber is embedded in the resin matrix, the critical buckling mode of the fiber will transform into sinusoidal due to the existence of shear strain energy in the resin matrix. And with the increase of temperature, the critical buckling wavelength of fiber will increase with the decrease of the modulus of resin matrix. Fig. 7 shows the wavelength of a single-CF reinforced SMPC at 100 °C as a function of E_m. It can be seen that with the increase of E_m, the critical buckling wavelength will decrease, but the decreasing rate will gradually slow down. The theoretical critical buckling wavelength proposal in this paper is in good agreement with the FEA results. However, the critical buckling wavelength calculated in this paper is larger than that obtained from Darby et al. [33], who also took into account the decay of strain in the resin matrix, and the critical buckling half-wavelength was calculated by.

$$\lambda_c = \pi r \sqrt[8]{\frac{{E_f}^2}{8GE_m}} \# \tag{74}$$

It can also be seen from Fig. 7 that the deviation between the critical buckling wavelengths calculated in this paper and proposed by Darby will increase with the decrease of E_m. So, the attenuation function proposed in this paper is more accurate when describing the attenuation phenomenon of strain in resin matrix, especially when E_m is small. Table 2 shows the critical buckling wavelengths of single-fiber

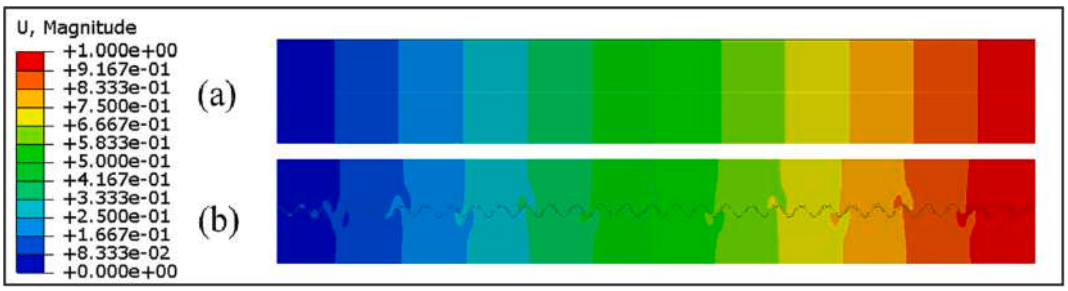

Fig. 8. The axial compressive displacement contours of single-CF reinforced composites calculated by Static Non-Linear Riks Method under the same compressive displacement at 100 °C **(a)** without initial imperfection, **(b)** with initial buckling mode-shape imperfection.

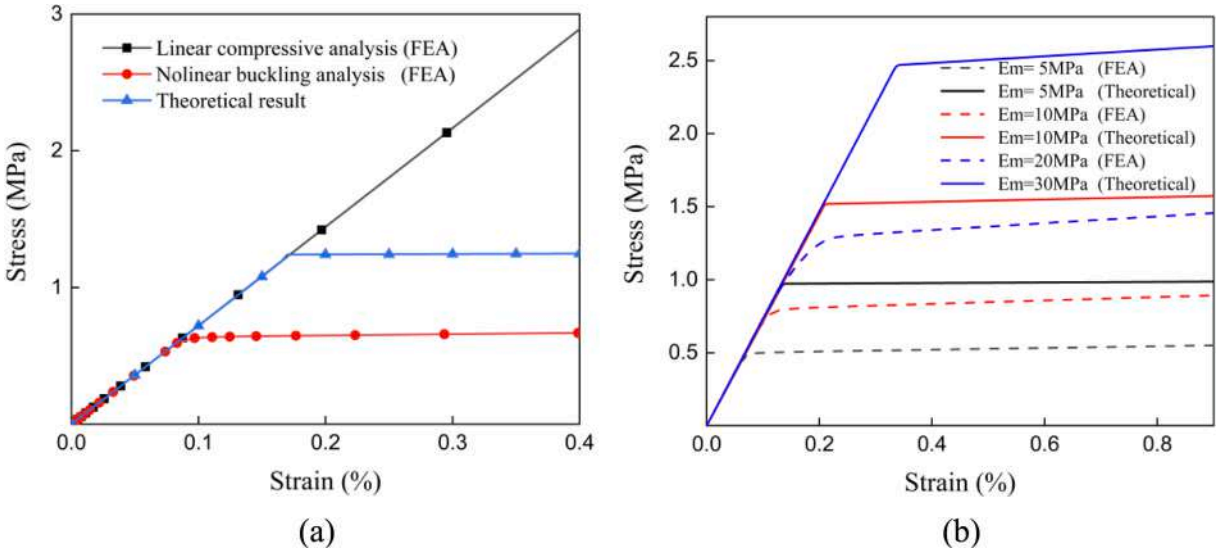

Fig. 9. The stress–strain curve of single-CF reinforced composites at 100 °C **(a)** FEA results and theoretical results at 100 °C, **(b)** FEA and theoretical results with different E_m.

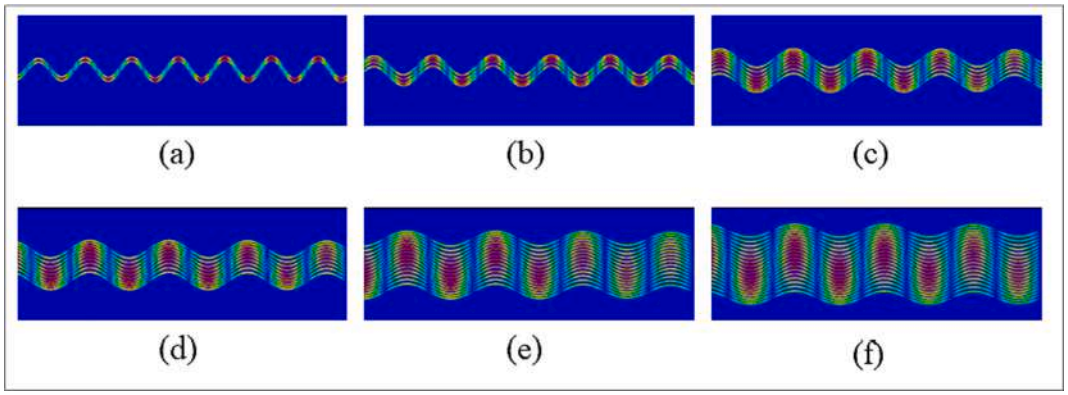

Fig. 10. The critical buckling modes (the Mises-stress contours) of multi-CF reinforced composite with the same fiber volume fraction $V_f = 10\%$ at 100 °C **(a)** 2 fibers, **(b)** 4fibers, **(c)** 8fibers, **(d)** 12 fibers, **(e)** 16fibers, **(f)** 20fibers.

reinforced composite from theoretical analysis and literatures. It can be seen that the experimental buckling wavelengths of single-fiber reinforced composite obtained from literatures fit well with the theoretical results. Therefore, the rationality and accuracy of the attenuation function $\chi(y)$ proposed in this paper are verified.

Then the nonlinear buckling process of single-CF reinforced composites under uniaxial compression is simulated by FEA. In this paper, the pseudo-dynamic method is used for analysis, and the brief introduction is described as follows: Firstly, the first-order buckling mode of the single-CF reinforced composite obtained from the above linear buckling analysis is multiplied by a scaling factor δ as the initial imperfection; Then, the initial imperfection is introduced into a perfect composite by modifying the coordinates of nodes using the inp. file of Abaqus; Finally, the Non-linear Riks Method is used for the following nonlinear buckling (post-buckling) analysis. The axial compressive displacement contours of single-CF reinforced composites (under the same compressive displacement at 100 °C) calculated by the Static Non-Linear Riks Method are shown in Fig. 8. Fig. 8(a) shows the

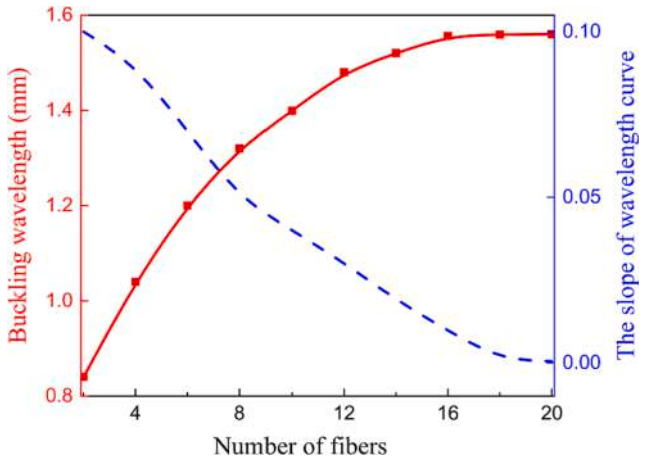

Fig. 11. The critical buckling wavelength of the CF reinforced composite with $V_f = 10\%$ at 100 °C as a function of the number of fibers and its slope curve.

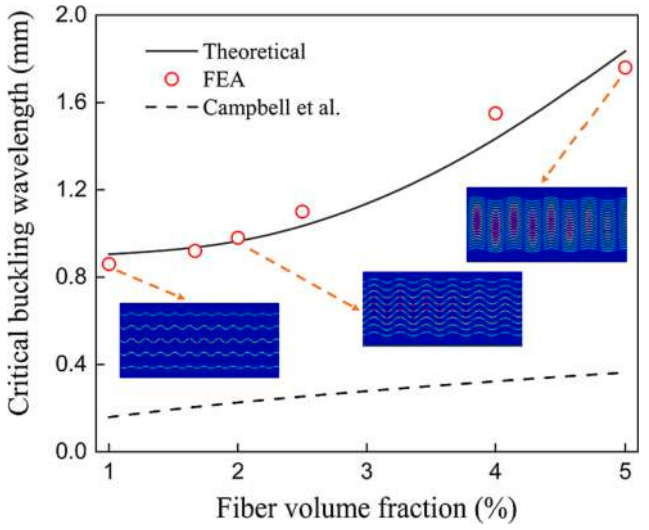

Fig. 12. The critical buckling wavelength of CF-reinforced composite at 100 °C as a function of V_f obtained from theoretical analysis, FEA and literature [31] and the corresponding typical critical buckling modes (the Mises-stress contours).

displacement contour where no initial imperfection is introduced, and it can be seen that no buckling deformation occurs in the fiber. Only when the initial buckling mode-shape imperfection is introduced, it is possible for the fiber to produce post-buckling deformation in the following Static Non-Linear Riks analysis, which can be seen in Fig. 8(b).

It can also be seen from Fig. 9(a) that if no initial imperfection is introduced, the stress of the single-CF reinforced composite under uniaxial compression will increase linearly with the strain, indicating that the fiber will not buckle, which is obviously inconsistent with the theoretical analysis results in this paper. With the introduction of the initial imperfection, we observe that the material deforms linearly before the strain reaches the critical buckling strain $\varepsilon_{critical}$. Once the strain reaches $\varepsilon_{critical}$, the fiber will buckle and its tangent modulus will decrease rapidly, so the composite will lose part of its load-bearing capacity. It can be seen that the tangent modulus of the material obtained by the theoretical and finite element results in the whole nonlinear buckling process is basically the same, whether before and after buckling. In addition, it can also be seen from Fig. 9(b) that with the change of E_m, the tangent moduli (before and after buckling) of the composite obtained by FEA and theoretical results are always the same. However, because imperfections are introduced in the Non-linear Riks analysis initially, the fiber will have premature buckling deformation, leading to the inaccuracy of the $\varepsilon_{critical}$ calculated by FEA, which will be smaller than that of the theoretical result. But we can see that the variation trend of $\varepsilon_{critical}$ obtained from FEA and theoretical analysis is the same with different E_m, indicating that the theoretical calculation method of post-buckling process in this paper is feasible and accurate. It is worth noting that the scaling factor in this section is equal to 1 % of the thickness of the shell, i.e., $\delta = 6.2 \times e^{-5}$.

3.2. Multi-fiber reinforced composite

When more fibers are embedded in the resin matrix, the buckling behavior will change. Therefore, before simulating the buckling behaviors of multi-fiber reinforced SMPC, the dimension parameters of the FEA model should firstly be determined. On the one hand, when establishing the finite element model, the fibers should theoretically cover the whole model completely. However, this will lead to the outermost fibers being too close to the boundary of the model, and the existence of boundary conditions will lead to inaccurate results, so the fibers should be as close to the center of the model as possible. On the other hand, when the fibers are too close to the center of the model, the excess resin outside the outermost fibers may also affect the deformation of the fibers. Therefore, before modeling multi-fiber reinforced composites, the optimal width of pure resin outside the outermost fibers in FEA model should be studied firstly to make the simulation results as accurate as possible.

The research object of this paper is unidirectional multi-fiber reinforced SMPC with the fiber volume fraction of less than 5 %. When the fiber volume fraction becomes higher, the effect of outermost resin width on the simulation results will be more severe, So, an "worst" situation should be studied to ensure the accuracy of the subsequent simulation results. As a result, we simulate the buckling behaviors of unidirectional multi-fiber reinforced composite with a fiber volume fraction of 10 %. As the number of fibers increases, the distance between the adjacent fibers remains constant, so the fiber volume fraction can be regarded as unchanged, and the width of pure resin outside the outermost fibers will decrease simultaneously. The mesh size will also not change as the number of fibers increases.

As can be seen from Fig. 10 and Fig. 11, with the increase of the number of fibers in the model, the width of pure resin outside the outermost fibers will decrease, and its buckling wavelength will increase significantly, up to 85.7 %, indicating that the width of pure resin outside the outermost fibers in the model does have a great influence on the simulation results. It can be seen from Fig. 11 that the slope of the wavelength curve is decreasing gradually with the increase of the number of fibers, and the buckling wavelength will gradually approach a stable value when the width of pure resin outside the outermost fibers is about 0.5 mm. It indicates that the result calculated by this model has already approached the accurate value. Continually increasing the number of fibers will only increase the calculation cost, but will not improve the accuracy of the results. In addition, if the fibers are too close to the model's boundary, they may also be affected by the boundary constraint conditions of the model. Therefore, in the subsequent simulation of multi-fiber reinforced composites, the width of the outermost resin is selected as 0.5 mm, and the fiber volume fractions are 1 %, 1.66 %, 2 %, 2.5 %, 4 % and 5 %, respectively. The fiber is carbon fiber, and the resin is shape memory epoxy resin at 100 °C, whose modulus is 7.2 MPa. For the accuracy of simulation, there should be at least four meshes between adjacent fibers, and the dimension of the whole model does not change with the change of fiber volume fractions.

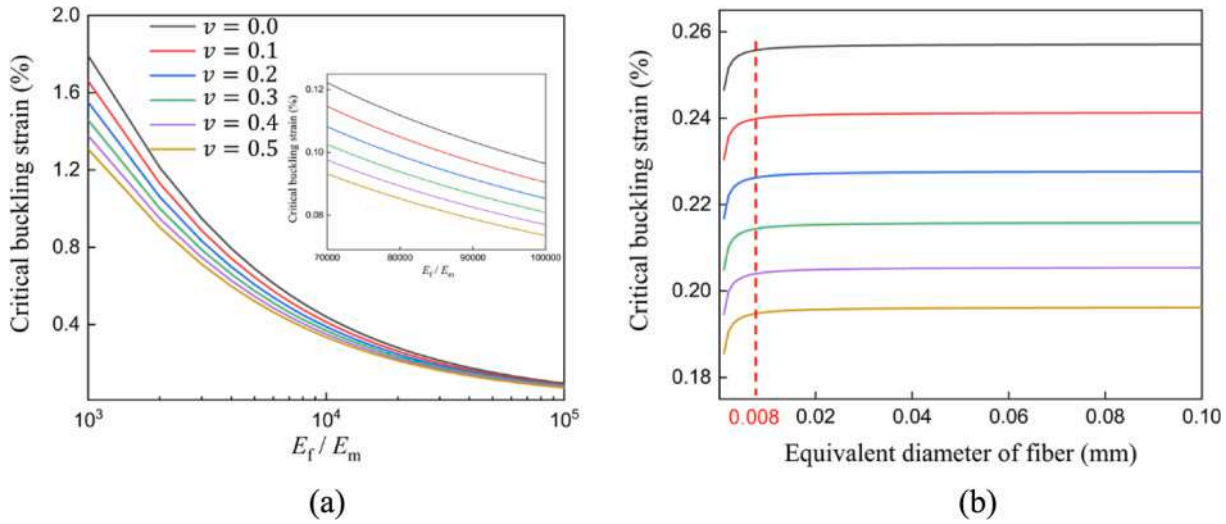

Fig. 13. The critical buckling strain of single-CF reinforced composite through theoretical calculation **(a)** $\varepsilon_{critical}$ as a function of E_f/E_m when d remains 6.2um, **(b)** $\varepsilon_{critical}$ as a function of d when E_f/E_m remains 23000.

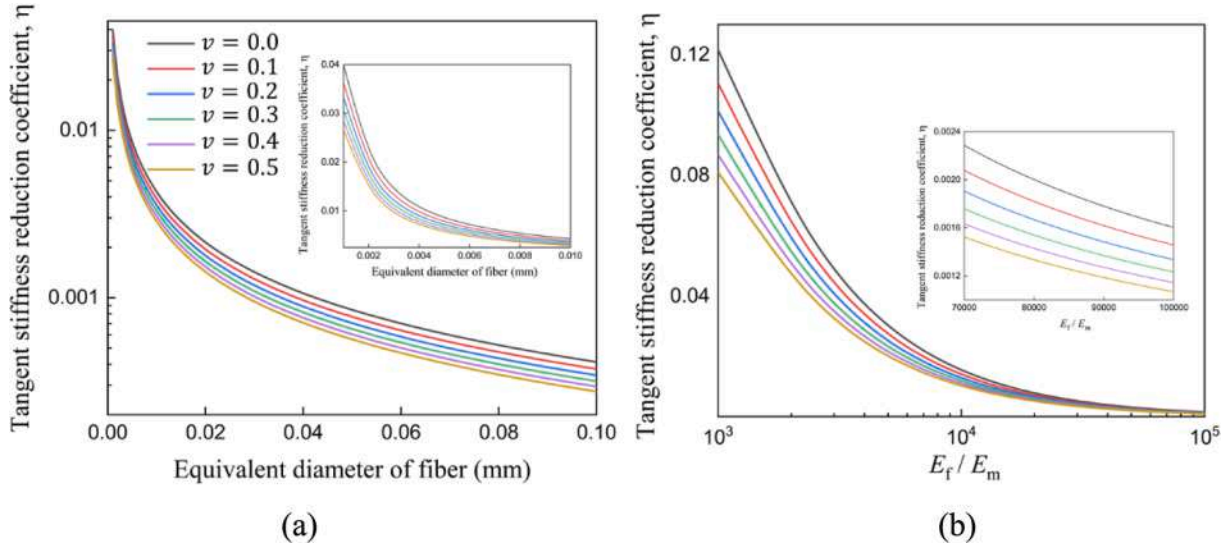

Fig. 14. The tangent stiffness reduction coefficient η of single-CF reinforced composite through theoretical calculation **(a)** η as a function of d when E_f/E_m remains 23000, **(b)** η as a function of E_f/E_m when d remains 6.2um.

Fig. 12 shows the first-order critical buckling modes and wavelengths of composites at 100 °C with different fiber volume fractions. It can be seen that the critical buckling wavelength will increase significantly with the increase of fiber volume fraction. As shown in Fig. 12, compared with the calculation results of Campbell et al. [31], the theoretical calculation results proposed in this paper are in better agreement with the FEA results. Thus, the theoretical model in this article can describe the buckling behaviors of unidirectional multi-fiber reinforced composite with low fiber volume fraction well.

4. Analysis of key parameters

4.1. Parameter study of single-fiber reinforced composite

E_f and E_m are important factors affecting the buckling behaviors of composites, which is not only reflected in the critical buckling strain, but also affects the nonlinear buckling behaviors. In addition, it can be seen from the theoretical results that the $\varepsilon_{critical}$ of single-fiber reinforced composites is not only related to the mechanical properties of fiber and resin, but also related to the fiber's equivalent diameter d. Therefore, the first step is to find out the influence of modulus ratios of fiber and resin E_f/E_m and the fiber's equivalent diameter d on $\varepsilon_{critical}$. It can be seen from Fig. 13(a) that when d and ν remain unchanged, $\varepsilon_{critical}$ will decrease with the increase of E_f/E_m. It indicates that the "softer" the resin is, the fiber is more prone to buckling, because the fiber will gain less deformation resistance from the matrix. It can also be seen from Fig. 13(b) that when E_f/E_m remains constant, $\varepsilon_{critical}$ will increase rapidly with the increase of d and then approaches a stable value. This bifurcation point will not change with ν, which remains stable at about 8um. In addition, $\varepsilon_{critical}$ will decrease with the increase of ν from 0 to 0.5, indicating that the incompressibility of the resin will reduce the critical buckling strain of the composite.

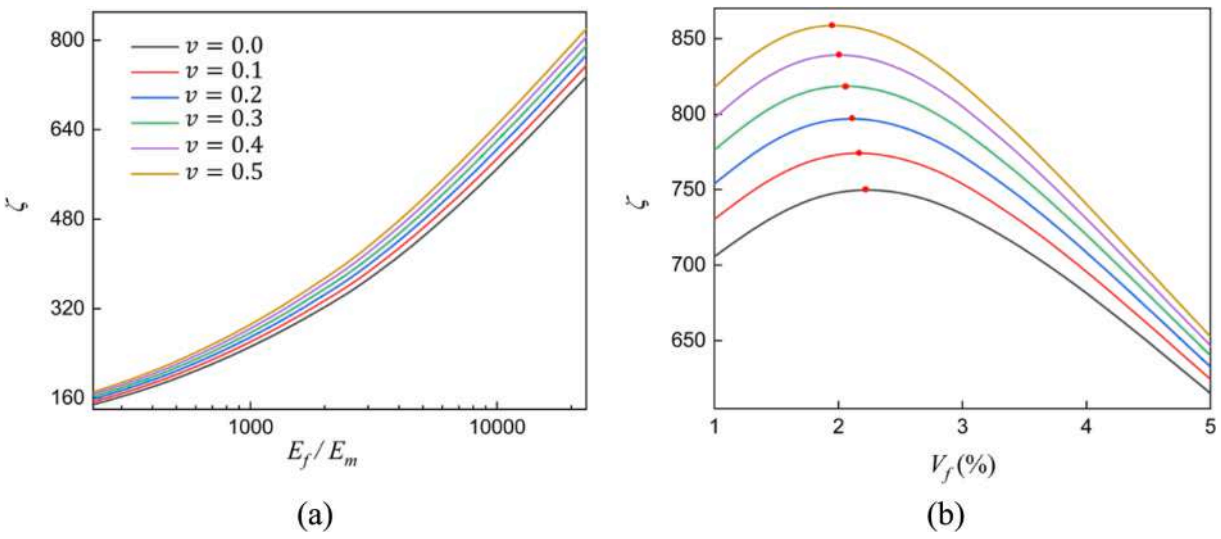

Fig. 15. The dimensionless parameter ζ of multi-fiber reinforced composite in critical buckling state through theoretical calculation **(a)** The dimensionless parameter ζ as a function of E_f/E_m when V_f remains 3%, **(b)** The dimensionless parameter ζ as a function of V_f when E_f/E_m remains 23000.

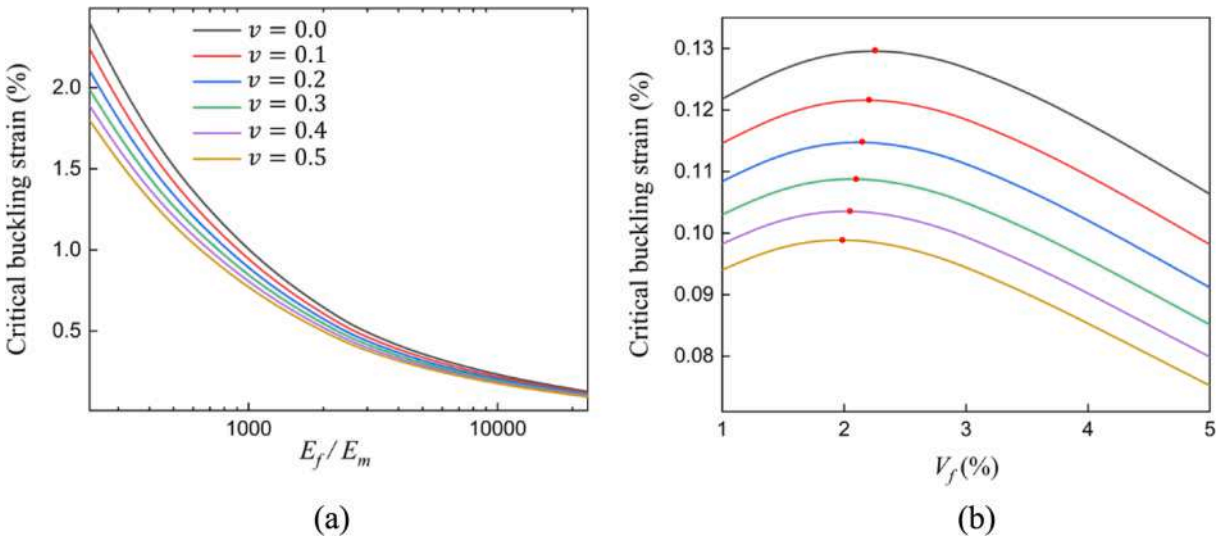

Fig. 16. The critical buckling strain $\varepsilon_{critical}$ of multi-fiber reinforced composite through theoretical calculation **(a)** $\varepsilon_{critical}$ as a function of E_f/E_m when V_f remains 3%, **(b)** $\varepsilon_{critical}$ as a function of V_f when E_f/E_m remains 23000.

It is worth noting that the tangent modulus of composite will decrease rapidly when microbuckling of fiber occurs, so the tangent stiffness attenuation coefficient η is introduced in this article to quantify this phenomenon, where η is equal to the ratio of the tangent modulus of composite after and before buckling. The lower the η is, the attenuation of tangent modulus of composite during buckling will be severer. It can be seen from Fig. 14(a) that when E_f/E_m remains constant at 23000, as d increases from 1um to 100um, the η will decrease significantly, even drop to 1 % of the initial value. As can be seen in Fig. 14(b), with the increase of E_f/E_m from 1000 to 23000, η will also decrease significantly. These phenomena indicate that the larger the fiber's diameter is or the softer the resin is, the more obvious the tangent stiffness attenuation of the composite will occur after buckling. In addition, η will decrease slightly with the increase of ν from 0 to 0.5, indicating that the incompressibility of the resin matrix will reduce the tangent stiffness attenuation coefficient of the composite after buckling.

4.2. Parameter study of multi-fiber reinforced composite

From the microbuckling analysis of multi-fiber reinforced composite, we derived the formula of the dimensionless parameter ζ, critical buckling strain $\varepsilon_{critical}$ and tangent stiffness reduction coefficient η in relation to E_f/E_m and V_f in Eq (57), (61) and (63). These prominent features of such multi-fiber reinforced composite will be analyzed hereafter. As can be seen in Eq (57), the dimensionless parameter ζ can reflect the variation rates of U_{m0} and U_f with ε to some extent, which is related to V_f and the mechanical properties of resin matrix and fiber. The influence of E_f/E_m and V_f on ζ can be analyzed by calculating the value of ζ in the critical buckling state. It can be seen in Fig. 15 that the dimensionless parameter ζ will increase with the increase of E_f/E_m. However, with the increase of V_f, ζ will not increase or decrease monotonically, but has a maximal value at a certain V_f. And with the

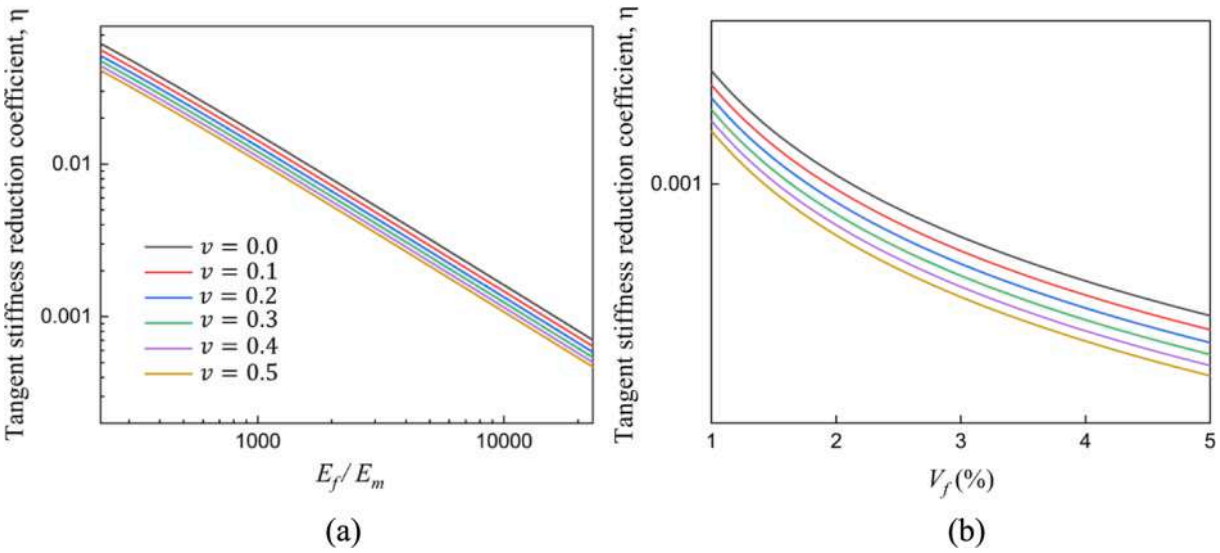

Fig. 17. The tangent stiffness reduction coefficient η of multi-fiber reinforced composite through theoretical calculation **(a)** η as a function of E_f/E_m when V_f remains 3%, **(b)** η as a function of V_f when E_f/E_m remains 23000.

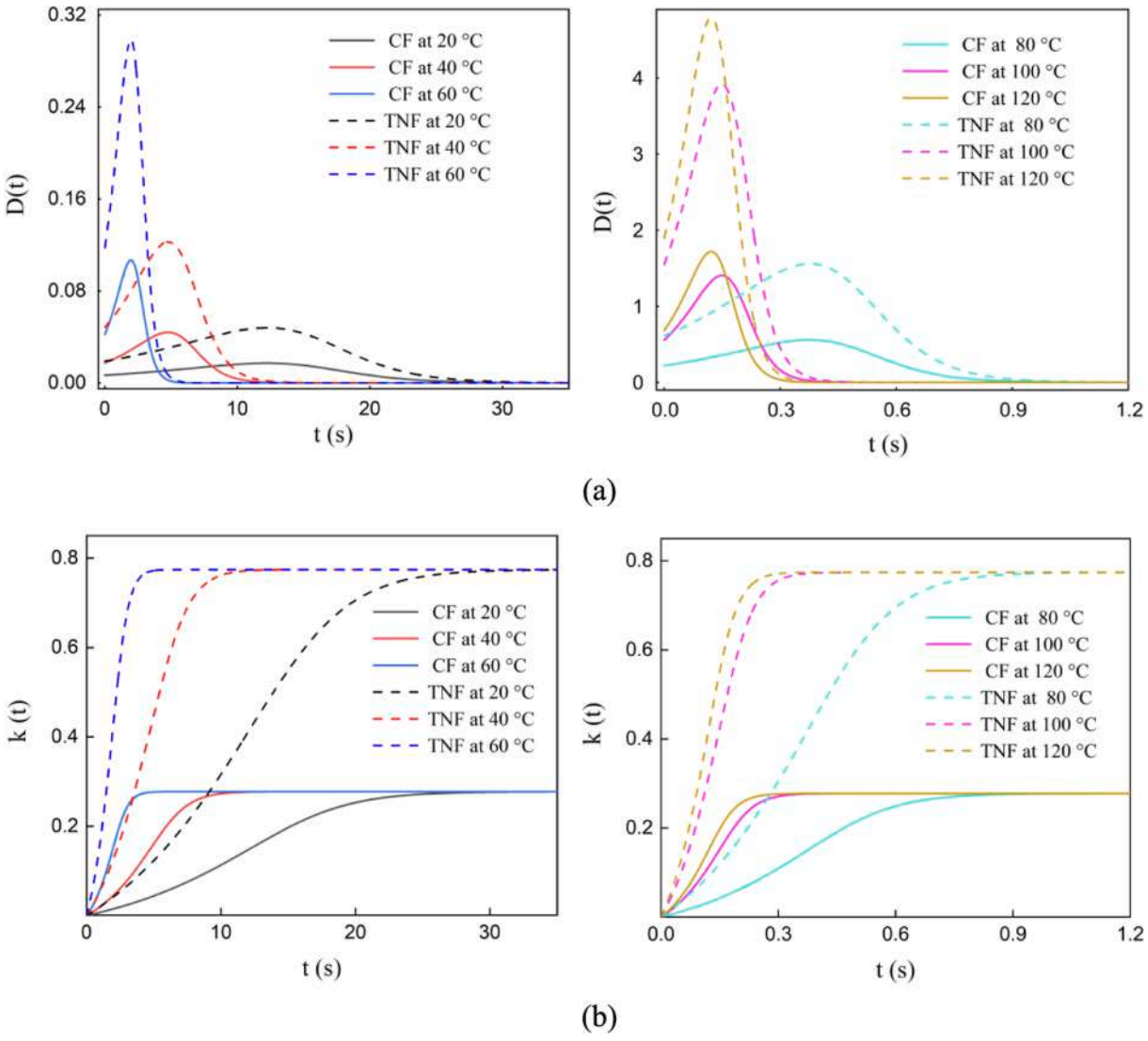

Fig. 18. The evolution of buckling wavelength with time at different temperatures **(a)** the rate of variation of buckling wavelength as a function of time, **(b)** the ratio of variation of buckling wavelength as a function of time.

increase of v from 0 to 0.5, the corresponding V_f at the bifurcation points will decrease slightly. It is worth noting that ζ will increase with the increase of v, that is, the incompressibility of the resin matrix will lead to the increase of the rates of variation of U_{m0} and U_f with respect to ε.

In order to describe the whole process of the nonlinear buckling behaviors of multi-fiber reinforced composite more intuitively, we need to study the critical buckling strain $\varepsilon_{critical}$ and the tangent stiffness attenuation coefficient η. It can be seen in Fig. 16(a) that $\varepsilon_{critical}$ will decrease significantly with the increase of E_f/E_m, indicating that the composite is more prone to undergo compressive buckling deformation when the resin matrix is "softer", which is obvious and easy to understand. However, with the increase of V_f, the variation trend of $\varepsilon_{critical}$ is different from the monotonically increasing trend of critical buckling wavelength, which will have a maximal value at a certain V_f as shown in Fig. 16(b). The main reasons for this phenomenon are as follows:

In the case of extremely sparse fibers ($V_f < 2\%$), with the increase of V_f, the distance of adjacent fibers will decrease consequently, and the buckling deformation of fibers embedded in the resin matrix will be "hindered" by the adjacent fibers, so the $\varepsilon_{critical}$ will increase as a consequence. However, as the fiber volume fraction continues to increase ($V_f > 2\%$), a continuous "zone" structure will be formed among fibers, which can be regarded as a whole section. As a result, the "hindered" effect between adjacent fibers will gradually decrease, so does the critical buckling strain. It can also be seen that when v increases from 0 to 0.5, the corresponding V_f at the bifurcation points will decrease slightly, indicating that the incompressibility of the resin matrix will make the "zone" structure among fibers easier to be formed, so that the $\varepsilon_{critical}$ will be smaller.

It can also be seen from Fig. 17 that with the increase of E_f/E_m and V_f, the tangent stiffness reduction coefficient η of the multi-fiber reinforced composite will decrease, indicating that the "softer" the resin is or the "denser" the fiber is, the more obvious stiffness degradation will occur on the composite after buckling. When v increases from 0 to 0.5, the η will decrease slightly, that is the incompressibility of the resin matrix will aggravate the stiffness degradation of composite after buckling.

4.3. Parameter study of viscoelastic composite

After obtaining the μ_∞, μ_1 and p_1 of shape memory epoxy resin at different temperatures from the isothermal stress relaxation experiments as shown in Section S2.2 (Supplemental File), the corresponding changing rate and changing ratio of buckling wavelength of single-fiber reinforced SMPC at different temperatures can be calculated. In this paper, $D(t) = d\lambda/dt$ is used to describe the changing rate of the buckling half-wavelength $\lambda(t)$, and $k(t)$ is used to describe the changing ratio of $\lambda(t)$, where.

$$k(t) = \frac{\lambda(t) - \lambda(0)}{\lambda(0)}\# \tag{75}$$

The curves of $D(t) - t$ and $k(t) - t$ of single CF and CNF reinforced SMPCs at different temperatures are shown in Fig. 18. As can be seen in Fig. 18(a), $D(t)$ will firstly increase over time and then rapidly converge to 0. It means that the buckling wavelength will increase rapidly with time and then converge to a stable value, which can also be seen in Fig. 18(b). Besides, the $D(t)$ of single-CF reinforced SMPC is lower than that of single-CNF reinforced SMPC at the same temperature, resulting in the increasing amount of buckling wavelength of single-CF reinforced SMPC lower than that of single-CNF reinforced SMPC. However, the type of fiber does not affect the convergence time, which is only related to temperature. The convergence time of $D(t)$ will be shorter at high temperature, so that $\lambda(t)$ will reach a stable state earlier.

5. Conclusion

This paper developed the microbuckling mechanical models of single-fiber and multi-fiber reinforced SMPC under pure compressive deformation. The critical buckling and post-buckling behaviors of unidirectional fiber-reinforced SMPC with low fiber volume fraction were investigated. We determined the strain energy expression of the SMPC thermodynamic system with the assumption of small deformation and the superposition principle. The attenuation of shear strain in the resin matrix was also taken into consideration. Based on the least-energy principle, we derived the attenuation function $\chi(y)$ and key parameters in the compressive deformation process of single-fiber and multi-fiber reinforced SMPC, including the critical buckling half-wavelength λ, critical buckling strain $\varepsilon_{critical}$. The stress–strain response and the tangent stiffness reduction coefficient η during the post-buckling process were also calculated.

The attenuation function and critical buckling half-wavelength proposed in this paper were in good agreement with the results from FEA and literatures. It was found that: (a) With the decrease of the wavelength of fiber, the attenuation rate of displacement in resin matrix would become faster. (b) With the increase of resin's modulus, λ would decrease, but the decreasing rate would gradually slow down; while the λ would increase significantly with the increase of fiber's volume fraction or diameter. (c) $\varepsilon_{critical}$ would decrease with the decrease of resin's modulus, while $\varepsilon_{critical}$ would increase rapidly with the increase of fiber's diameter and then approach a stable value; with the increase of fiber's volume fraction, $\varepsilon_{critical}$ would not increase monotonically, but have a maximal value at a certain V_f; besides, the incompressibility of the resin would reduce the critical buckling strain of the SMPC. (d) The larger the fiber's diameter or volume fraction was, or the softer the resin was, the more obvious the tangent stiffness attenuation of the composite would occur after buckling; the incompressibility of the resin matrix would also reduce η of the composite after buckling.

The classical elastic–viscoelastic correspondence principle was then established to solve the evolvement rule of the microbuckling wavelength of single-CF and CNF reinforced SMPC with temperature and time. It was found that the buckling wavelength would increase rapidly with time and then converge to a stable value, and the increasing amount of buckling wavelength of single-CF reinforced SMPC was lower than that of single-CNF reinforced SMPC. However, the type of fiber did not affect the convergence time, which was only related to temperature. The convergence time would be shorter at high temperature, so that λ will reach a stable state earlier.

Declaration of Competing Interest

The authors declare that they have no known competing financial interests or personal relationships that could have appeared to influence the work reported in this paper.

Data availability

Data will be made available on request.

Acknowledgements

The authors would like to thank for the Heilongjiang Touyan Innovation Team Program. This work is supported by the National Natural Science Foundation of China (Grant No. 11632005, 11872020).

Appendix A

The Mises-stress contours of pure fiber and single-CF and CNF reinforced composites at different temperatures are shown in Fig. A1.

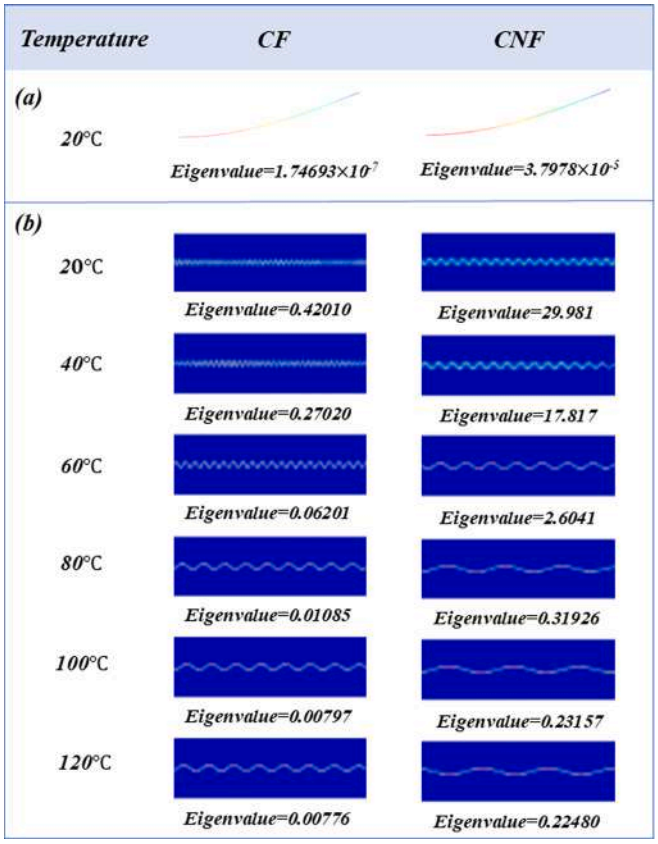

Fig. A1. The Mises-stress contours of the critical buckling modes at different temperatures **(a)** the pure single CF and CNF at 20 °C, **(b)** single-CF/CNF reinforced SMPC at different temperatures.

Appendix B. Supplementary material

Supplementary data to this article can be found online at https://doi.org/10.1016/j.compstruct.2022.115975.

References

[1] Lin L, Zhou Q, Li M. A thermally and electrically shape memory polymer prepared by a novel electro-mixed fusion preparation method. Mater Lett 2019;256:126574. https://doi.org/10.1016/j.matlet.2019.126574.

[2] Spiegel CA, Hackner M, Bothe VP, Spatz JP, Blasco E. 4D Printing of Shape Memory Polymers: From Macro to Micro. Adv Funct Mater 2022;2110580.

[3] Li F, Fabrizio S, Lan X, Liu L, Liu Y, Leng J. Bending shape recovery of unidirectional carbon fiber reinforced epoxy-based shape memory polymer composite. Compos Part A-Appl S 2019;116:167–79.

[4] Huang X, Mahyar P, Dong K, Li R, Chen T, Xiao X. Tracing evolutions in electro-activated shape memory polymer composites with 4D pringting strategies: A systematic review. Compos Part A-Appl S 2021;147:106444.

[5] Mattmann M, De Marco C, Briatico F, Tagliabue S, Colusso A, Chen X-Z, et al. Thermoset Shape Memory Polymer Variable Stiffness 4D Robotic Catheters. Adv Sci 2022;9(1):2103277. https://doi.org/10.1002/advs.v9.110.1002/advs.202103277.

[6] Wang X, Liu Y, Lu H, Wu N, Hui D, Fu Y-Q. A coupling model for cooperative dynamics in shape memory polymer undergoing multiple glass transitions and complex stress relaxations. Polym 2019;181:121785. https://doi.org/10.1016/j.polymer.2019.121785.

[7] Liu R, Li Y, Liu Z. Experimental study of thermo-mechanical behavior of a thermosetting shape-memory polymer. Mech Time-Depend Mat 2019;23(3):249–66.

[8] Liu Y, Gall K, Dunn ML, Greenberg AR, Diani J. Thermomechanics of shape memory polymers: uniaxial experiments and constitutive modeling. Int J Plasticity 2006;22(2):279–313.

[9] Cortés A, Cosola A, Sangermano M, Campo M, González Prolongo S, Pirri CF, et al. DLP 4D-Printing of Remotely, Modularly, and Selectively Controllable Shape Memory Polymer Nanocomposites Embedding Carbon Nanotubes. Adv Funct Mater 2021;31(50):2106774. https://doi.org/10.1002/adfm.v31.5010.1002/adfm.202106774.

[10] Tan Q, Liu L, Liu Y, Leng J. Thermal mechanical constitutive model of fiber reinforced shape memory polymer composite: based on bridging model. Compos Part A-Appl S 2014;64:132–8.

[11] Lu H, Liu Y, Gou J, Leng J, Du S. Synergistic effect of carbon nanofiber and carbon nanopaper on shape memory polymer composite. Appl Phys Lett 2010;96(8):084102. https://doi.org/10.1063/1.3323096.

[12] Lu H, Yu K, Sun S, Liu Y, Leng J. Mechanical and shape-memory behavior of shape-memory polymer composites with hybrid fillers. Polym Int 2010;59(6):766–71.

[13] Su X, Peng X. A lamination model for shape memory polymer/woven fabric composites. Int J Comput Mater Sci Eng 2019;08(02):1950004. https://doi.org/10.1142/S2047684119500040.

[14] Leng J, Lan X, Liu Y, Du S. Shape-memory polymers and their composites: stimulus methods and applications. Prog Mater Sci 2011;56(7):1077–135.

[15] Liu Z, Hao S, Lan X, Bian W, Liu L, Li Q, et al. Thermal design and analysis of a flexible solar array system based on shape memory polymer composites. Smart Mater Struct 2022;31(2):025021. https://doi.org/10.1088/1361-665X/ac40df.

[16] Li F, Liu Y, Leng J. Progress of shape memory polymers and their composites in aerospace applications. Smart Mater Struct 2019;28(10):103003. https://doi.org/10.1088/1361-665X/ab3d5f.

[17] Lan X, Liu Y, Lv H, Wang X, Leng J, Du S. Fiber reinforced shape-memory polymer composite and its application in a deployable hinge. Smart Mater Struct 2009;18(2):024002. https://doi.org/10.1088/0964-1726/18/2/024002.

[18] Gall K, Mikulas M, Munshi N, Beavers F, Tupper M. Development and Testing of a Hinge/Actuator Incorporating Elastic Memory Composites. AIAA 2003;1496.

[19] Yuan T, Yang Yi, Kong X, Wu W. Similarity criteria for the buckling process of stiffened plates subjected to compressive load. Thin Wall Struct 2021;158:107183. https://doi.org/10.1016/j.tws.2020.107183.

[20] Jochum Ch, Grandidier J-C. Microbuckling elastic modelling approach of a single carbon fibre embedded in an epoxy matrix. Compos sci technol 2004;64(16):2441–9.

[21] Mechin P-Y, Keryvin V, Grandidier J-C, Glehen D. An experimental protocol to measure the parameters affecting the compressive strength of CFRP with a fibre micro-buckling failure criterion. Compos Struct 2019;211:154–62.

[22] Dow NF, Gruntfest IJ. Determination of most needed potentially possible improvements in materials for ballistic and space vehicles. General Electric Co: Space Science Laboratory, TJS R; 1960. p. 60.

[23] Greszczuk LB. On failure modes of unidirectional composites under compressive loading. In: Sih GC, Tamuzs VP, editors. Fracture of Composite Materials. Dordrecht: Springer Netherlands; 1982. p. 231–44. https://doi.org/10.1007/978-94-009-7609-2_19.

[24] Rosen B. Mechanics of Composite Strengthening, in" Fiber Composite Materials", published by American Society for Metals. Ohio: Metals Park; 1965.

[25] De Morais AB. Prediction of the layer longitudinal compression strength. J compos mater 2000;34(21):1808–20.

[26] Lo KH, Chim E-S-M. Compressive strength of unidirectional composites. J Reinf Plast Comp 1992;11(8):838–96.

[27] Xu YL, Reifsnider KL. Micromechanical modeling of composite compressive strength. Journal of Comp Mater 1993;27(6):572–88.

[28] Basu S, Waas A, Ambur D. Compressive failure of fiber composites under multi-axial loading. J Mech Phys Solids 2006;54(3):611–34.

[29] Bednarcyk BA, Aboudi J, Arnold SM. The effect of general statistical fiber misalignment on predicted damage initiation in composites. Compos Part B-Eng 2014;66:97–108.

[30] Li Y, Stier B, Bednarcyk B, Simon J-W, Reese S. The effect of fiber misalignment on the homogenized properties of unidirectional fiber reinforced composites. Mech Mater 2016;92:261–74.

[31] Campbell D, Maji A. Failure mechanisms and deployment accuracy of elastic-memory composites. J Aerospace Eng 2006;19(3):184–93.

[32] Zhang J, Dui G, Liang X. Revisiting the micro-buckling of carbon fibers in elastic memory composite plates under pure bending. Int J Mech Sci 2018;136:339–48.

[33] Darby MI, Kanellopoulos VN. Theory of fibre buckling in carbon-fibre reinforced plastics. J Phys D Appl Phys 1987;20(3):298–302.

[34] Zhao Y, Li J, Cao YP, Feng X-Q. Buckling of an elastic fiber with finite length in a soft matrix. Soft Matter 2016;12(7):2086–94.